PHYSICAL REVIEW B **83**, 220402(R) (2011)

Exceptionally strong magnetism in the 4*d* perovskites $R\mathrm{TcO_3}$ (R = Ca, Sr, Ba)

C. Franchini,[1,2,*] T. Archer,[3] Jiangang He,[1] Xing-Qiu Chen,[2] A. Filippetti,[4] and S. Sanvito[3]

[1]*University of Vienna, Faculty of Physics and Center for Computational Materials Science, A-1090 Vienna, Austria*

[2]*Shenyang National Laboratory for Materials Science, Chinese Academy of Science, Shenyang, China*

[3]*School of Physics and CRANN, Trinity College, Dublin 2, Ireland*

[4]*CNR-IOM, UOS Cagliari, Dipartimento di Fisica, Universitá di Cagliari, I-09042 Monserrato (CA), Italy*

(Received 27 May 2011; published 13 June 2011)

The evolution of the magnetic ordering temperature of the $4d^3$ perovskites $R\mathrm{TcO_3}$ (R = Ca, Sr, Ba) and its relation with its electronic and structural properties has been studied by means of hybrid density functional theory and Monte Carlo simulations. When compared to the most widely studied 3*d* perovskites the large spatial extent of the 4*d* shells and their relatively strong hybridization with oxygen weaken the tendency to form Jahn-Teller like orbital ordering. This strengthens the superexchange interaction. The resulting insulating G-type antiferromagnetic ground state is characterized by large superexchange coupling constants (26–35 meV) and Neél temperatures (750–1200 K). These monotonically increase as a function of the R ionic radius due to the progressive enhancement of the volume and the associated decrease of the cooperative rotation of the $\mathrm{TcO_6}$ octahedra.

DOI: 10.1103/PhysRevB.83.220402 PACS number(s): 75.47.Lx, 71.15.Mb, 75.30.Et, 75.50.Ee

Intermediately located between manganese and rhenium, technetium ($5s^24d^5$) shares with its isovalent neighbors the intriguing possibility to form oxides with a complex structural, electronic, and magnetic phase diagram. However, the rare occurrence of natural Tc (Tc is essentially an artificial product of fission reactions) and the related radioactive risks (Tc is the lightest radioactive element, whose most abundant isotope, ^{99}Tc, decays with a half-life of 10^5 years), have made investigations of Tc-based oxides very sparse.[1–6] Overcoming these difficulties, Avdeev *et al.*[5] and Rodriguez *et al.*[6] have recently reported the successful synthesis of fabricated Tc-based perovskites, namely $\mathrm{CaTcO_3}$ and $\mathrm{SrTcO_3}$. Furthermore, they have shown that these compounds display the anomalously high Neél temperatures (T_N) of 800 K for $\mathrm{CaTcO_3}$ and 1000 K for $\mathrm{SrTcO_3}$, by far the highest among materials not incorporating 3*d* transition metals. These results are surprising and challenge our understanding of the magnetic interaction in perovskites. In particular, they pose three fundamental questions: (i) Is the origin of such a large magnetic ordering temperature related to the strong Tc 4*d*-O *p* hybridization?, (ii) What is the role played by the structural degrees of freedom? and (iii) Is the enhancement of T_N on Ca→Sr substitution related to the observed increase in unit cell volume and the corresponding modification of the internal atomic positions[7,8]?

In the present letter, by using a combination of hybrid density functional theory[9] and Monte Carlo (MC) simulations,[10] we address these issues at the microscopic level through a systematic study of the series $R\mathrm{TcO_3}$ (R = Ca, Sr, Ba). Our aim here is twofold. First, we wish to interpret and understand the experimental findings for $\mathrm{CaTcO_3}$ and $\mathrm{SrTcO_3}$, which can be only captured by beyond-local density functional theory (DFT), due to the incorrect treatment of the residual exchange-correlation effects still present in 4*d* compounds.[11] Second, we anticipate the experiments predicting the properties of the technetiates series end member $\mathrm{BaTcO_3}$.

We have employed the Heyd-Scuseria-Ernzerhof (HSE)[12] scheme as implemented in the VASP code[13–16] using a 4×4×4 *k*-points set, a cutoff energy of 300 eV, a mixing parameter of $a = 0.1$,[17] and standard structural optimization conditions.[18]

$R\mathrm{TcO_3}$ compounds adopt the same distorted *Pnma* perovskite structure as $\mathrm{LaMnO_3}$,[19] characterized by a $\mathrm{GdFeO_3}$-like (GFO) tilting of the $\mathrm{TcO_6}$ octahedra caused by the R-O and R-Tc covalencies, and a concomitant Jahn-Teller (JT) Tc-O bond length disproportionation, with long (l) and short (s) Tc-O2 in-plane distances and medium (m) Tc-O1 vertical ones (see Fig. 1 and Table I). When compared to $\mathrm{LaMnO_3}$, the experimental values of the JT modes $Q_2 = 2(l-s)/\sqrt{(2)}$ and $Q_3 = 2(2m-l-s)/\sqrt{(6)}$ in $\mathrm{CaTCO_3}$ and $\mathrm{SrTCO_3}$ (see Table I) are significantly smaller due to the intrinsically different electronic configuration of the transition metal ions. In $\mathrm{LaMnO_3}$ the Mn^{3+} ions 3*d* states are in a $t_{2g}^3e_g^1$ configuration and a strong JT effect is required to release the degeneracy of the e_g orbitals and to form an orbitally ordered state.[21] In contrast, in $R\mathrm{TcO_3}$ the Tc^{4+} ions ($4d^3$: $t_{2g}^3e_g^0$) have completely filled (empty) $t_{2g}(e_g)$ manifolds, similarly to Mn^{4+} ions in $\mathrm{CaMnO_3}$[22], a configuration that inhibits the occurence of electronic and structural JT instabilities and leads to an insulating G-type antiferromagnetic (AFM-G) ground state.[23] However, at variance with 3*d* transition metal (TM) ions in perovskites, where d^3 configurations unavoidably lead to fully polarized $m = 3\ \mu_B$ moments on TM (e.g., $\mathrm{CaMnO_3}$), here due to the much larger extension of the 4*d* electrons and in turns a much stronger hybridizations with O *p* states, a sizable amount of charge fills the 4*d* minority states as well, with a consequential reduction of magnetic moment and an overtly evident intra-atomic Hund's rule violation.

The structural parameters obtained by a full geometry optimization for the AFM-G ground state (Table I) are in excellent agreement with the available low-temperature experimental data and the overall relative error is smaller than 1%. The Tc-O2 distances in $\mathrm{SrTcO_3}$ are the only exceptions since a deviation of almost 2% is observed. Note that, at variance with $\mathrm{CaTcO_3}$, in $\mathrm{SrTcO_3}$, experiment finds an appreciable planar bond length anisotropy, i.e., the two Tc-O2 bond lengths differ by about 0.07 Å(at 3 K).[6,20] This appears quite anomalous if one considers that the 5% volume expansion associated to the substitution of Ca with the heavier Sr is expected to induce the quenching of the cooperative Q_2

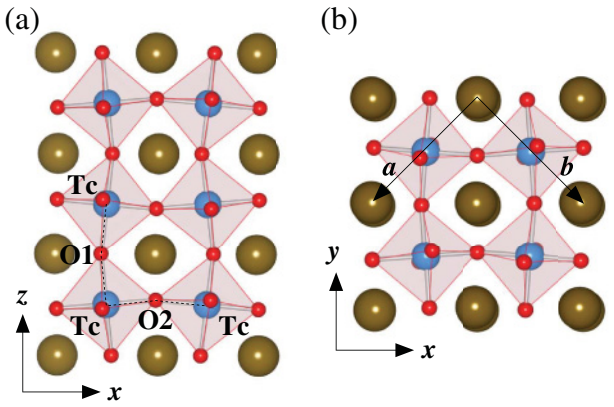

FIG. 1. (Color online) Side (a) and top (b) views of the *Pnma* structure of the distorted perovskite $R\mathrm{TcO_3}$. The Tc atoms [medium (light-blue) spheres] are surrounded by O_6 octahedran delimited by full (red) lines. The R atoms are represented by big (dark green) spheres. Both the conventional (abc) and Cartesian (xyz) coordinate systems are shown. In (a) a schematic representation (dashed lines) of the distorted Tc-O subnetwork indicating the Tc-O1-Tc and Tc-O2-Tc superexchange paths is given, where O1 and O2 are the apical and planar oxygen atoms, respectively.

and Q_3 JT modes. This translates in a reduction of the Tc-O disproportionation, similarly to the trend observed in the most widely study $R\mathrm{MnO_3}$ series.[7,8,24] The relatively strong Tc-O2 bond length anisotropy found in the experiments is comparable to that found in $\mathrm{LaMnO_3}$ and would suggest the presence of an orbitally ordered state in $\mathrm{SrTcO_3}$. This is unexpected for a 4*d* perovskite, given the abovementioned extendend character

TABLE I. Comparison between the low temperature (3 K)[20] experimental and calculated structural parameters for the G-type-oriented $R\mathrm{TcO_3}$ family. The corresponding cooperative Jahn-Teller local modes $Q_2 = 2(l-s)/\sqrt{(2)}$ and $Q_3 = 2(2m-l-s)/\sqrt{(6)}$ are also reported. In the definition, l, s, and m indicate the three inequivalent long (Tc-O2^l), short (Tc-O2^s), and medium (Tc-O1) Tc-O distances, respectively. Room temperature experimental data for $\mathrm{CaTcO_3}$ and $\mathrm{SrTcO_3}$ are from Refs. 5 and 6, respectively. No experimental data are available for $\mathrm{BaTcO_3}$. As a reference we report here the relevant experimental structural data for the prototypical JT/GFO compound $\mathrm{LaMnO_3}$: $Q_2 = 0.398$, $Q_3 = -0.142$, Mn $-\widehat{\mathrm{O1}}-$ Mn $= 154.3$, Mn $-\widehat{\mathrm{O2}}-$ Mn $= 156.7$, Mn-O2^l $= 2.184$, Mn-O2^s $= 1.903$, and Mn-O$_1$ $= 1.957$.[19]

	$\mathrm{CaTcO_3}$		$\mathrm{SrTcO_3}$		$\mathrm{BaTcO_3}$
	Expt.	HSE	Expt.	HSE	HSE
a (Å)	5.526	5.527	5.543	5.559	5.678
b (Å)	7.695	7.695	7.854	7.856	8.038
c (Å)	5.389	5.386	5.576	5.592	5.688
V (Å^3)	229.15	229.04	242.74	244.20	259.59
Tc $-\widehat{\mathrm{O1}}-$ Tc (°)	150.43	150.52	161.57	164.74	178.89
Tc $-\widehat{\mathrm{O2}}-$ Tc (°)	151.53	150.84	166.96	168.76	179.22
Tc-O2^l (Å)	2.002	1.998	2.015	1.983	2.010
Tc-O2^s (Å)	1.990	1.993	1.942	1.979	2.010
Tc-O1 (Å)	1.985	1.988	1.990	1.981	2.010
Q_2	0.017	0.007	0.103	0.005	0.000
Q_3	−0.018	−0.012	0.018	0.001	0.000

TABLE II. Compilation of measured and calculated magnetic moment m, exchange coupling constants T_N and relative stability of the different magnetic phases considered [$\Delta E_{GC} = E(\mathrm{AFM}-C) - E(\mathrm{AFM}-G)$, $\Delta E_{GA} = E(\mathrm{AFM}-A) - E(\mathrm{AFM}-G)$, and $\Delta E_{GF} = E(\mathrm{FM}) - E(\mathrm{AFM}-G)$] for $R\mathrm{TcO_3}$ (R = Ca, Sr, and Ba). Experimental data (m, taken at 4 K, and T_N) are available only for $\mathrm{CaTcO_3}$[5] and $\mathrm{SrTcO_3}$.[6]

	$\mathrm{CaTcO_3}$		$\mathrm{SrTcO_3}$		$\mathrm{BaTcO_3}$
	Expt.	Calc.	Expt.	Calc.	Calc.
m (μ_B)	∼2.0	2.10	2.13	2.04	2.04
ΔE_{CG} (meV/f.u.)	–	81	–	121	139
ΔE_{AG} (meV/f.u.)	–	191	–	289	299
ΔE_{FG} (meV/f.u.)	–	313	–	449	439
J_1 (meV)	–	−26.2	–	−35.3	−34.0
J_2 (meV)	–	−1.3	–	−0.7	0.1
T_N (K)	800	750	1020	1135	1218

of the 4*d* manifold. On the other hand, HSE yields a Tc-O2 bond length anisotropy smaller for $\mathrm{SrTcO_3}$ (0.005) than for $\mathrm{CaTcO_3}$ (0.007), thus drawing a globally consistent picture. Our results describe clear trends going from small (Ca) to large (Ba) cation size: The increase of volume, the stretching of Tc $-\widehat{\mathrm{O}}-$ Tc bond angles, the consequential decrease of tilting distortion, and the quenching of the Q_2 mode, which controls the relative difference between the in-plane Tc-O2 bond lengths. How these subtle structural properties affect the magnetism and how they can explain the observed surprisingly large T_N is discussed next.

By mapping the HSE total energies for different magnetic configurations onto a Heisenberg Hamiltonian (for unitary spins) we have evaluated the nearest-neighbor (NN, J_1) and next-nearest-neighbor (NNN, J_2) magnetic exchange parameters as a function of the ionic radius r_R.[25] The results are summarized in Table II. The NN superexchange (SE) Tc-O-Tc path, as illustrated in Fig. 1, connects NN Tc atoms via planar (Tc-O2-Tc) and apical (Tc-O1-Tc) oxygen atoms. Because of the almost identical Tc-O distances and Tc $-\widehat{\mathrm{O}}-$ Tc angles (see Table I) we have found that the in-plane ($J_1^{\parallel}$) and out-of-plane ($J_1^{\perp}$) values of J_1 are equal, both in sign (thus establishing the AFM-G ordering) and magnitude (within 10^{-1} meV). Therefore, we have finally adopted an effective Hamiltonian, including an isotropic J_1 magnetic interaction.

In addition to the ferromagnetic (FM) alignment three additional AFM configurations have been considered in fitting the J's: AFM-A [(100) planes of like spins alternating along the c axis], AFM-C (antiferromagnetic order in the xy plane with a ferromagnetic order along z), and AFM-G (all spins are antiferromagnetically coupled to their nearest neighbors). At variance with what found with conventional local DFT functionals,[5,6] HSE provides very stable magnetic solutions for every spin ordering with almost identical values of the magnetic moment of Tc ($\approx 2\ \mu_B$; see Table II). Furthermore, the AFM-G phase turns out to be the most stable (see Table II). The Heisenberg Hamiltonian is then used to evaluate T_N via MC calculations.[26] Note that in doing that we have rescaled the J's by a factor $S^2/S(S+1)$ ($S = 3/2$),

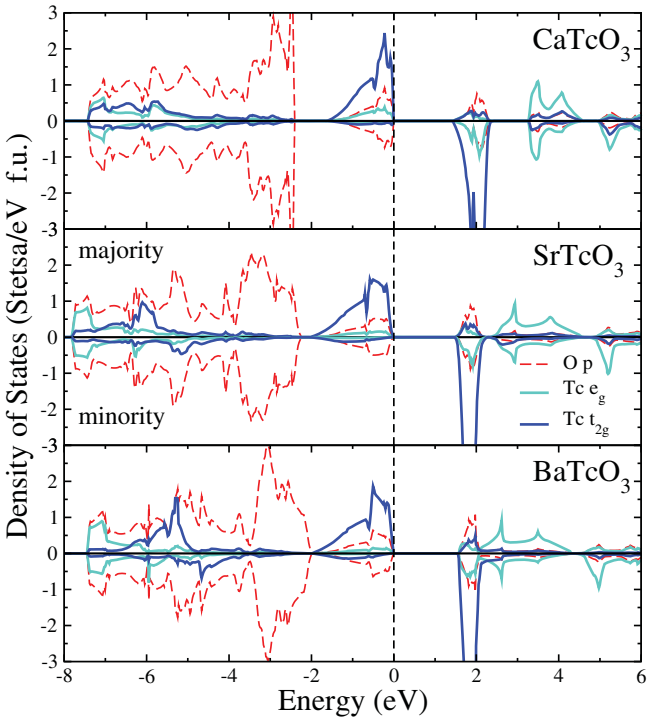

FIG. 2. (Color online) HSE calculated density of states for the $R\mathrm{TcO_3}$ series in the G-type AFM ground state decomposed over majority and minority O p and Tc t_{2g} and e_g states. The calculated band gaps are 1.4 eV ($\mathrm{CaTcO_3}$), 1.48 eV ($\mathrm{SrTcO_3}$), and 1.57 eV ($\mathrm{BaTcO_3}$).

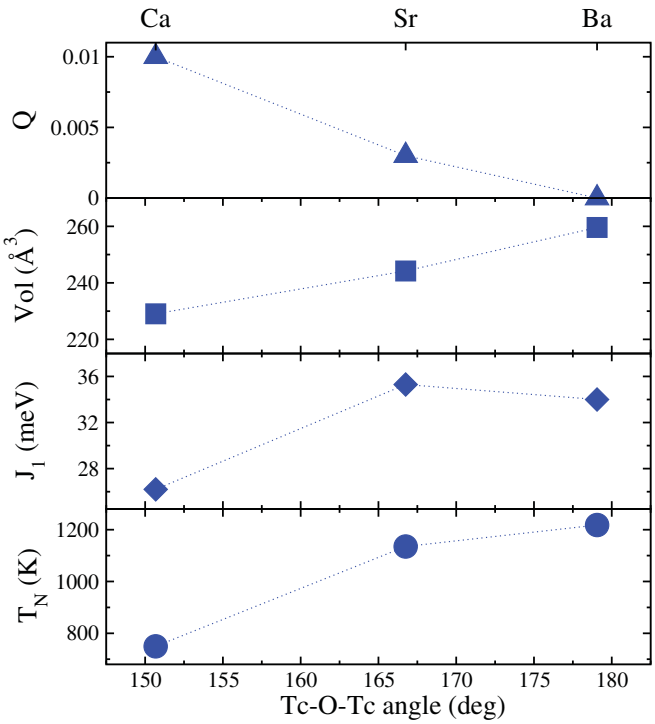

FIG. 3. (Color online) Dependency of the relevant magnetic (T_N and J_1) and structural [volume and $Q = 1/2(Q_1 + Q_2)$] quantities on the Tc $-\widehat{\mathrm{O}}-$ Tc angle (average between Tc $-\widehat{\mathrm{O1}}-$ Tc and Tc $-\widehat{\mathrm{O2}}-$ Tc) in the $R\mathrm{TcO_3}$ series.

which accounts for quantum fluctuations.[27] The results are summarized in Table II. The calculated T_N for $\mathrm{CaTcO_3}$ (750 K) and $\mathrm{SrTcO_3}$ (1135 K) are in very good agreement with experiments and the T_N predicted for $\mathrm{BaTcO_3}$ (1218 K), if experimentally confirmed, would represent the highest magnetic ordering temperature for any system without 3*d* states.

These unexpectedly large magnetic ordering temperatures can be understood in the framework of Anderson's theory of SE interactions,[28] which links the strength of the SE coupling constant with the actual hybridization between the metal and the mediating atom, and Van Vleck's theory of antiferromagnetism,[29] which connects the strength of the SE interaction with the magnetic ordering temperature. The calculated interatomic NN and NNN coupling constants listed in Table II show that the antiferromagnetic NN J_1 is the dominating parameter (~ -30 meV) and that it is almost two orders of magnitude larger than J_2 (~ -0.5 meV). The calculated density of states (DOS) displayed in Fig. 2 shows that these huge J_1 value arises from the strong covalency between the Tc t_{2g} and O p orbitals evolving along the wide 4*d* t_{2g} manifold, in particular for the topmost valence states spreading from $-1.5/2$ eV to the Fermi level (E_F). The increasing bandwidth (w) of this group of hybridized bands observed when going from $\mathrm{CaTcO_3}$ ($w = 1.5$ eV) to $\mathrm{SrTcO_3}$ and $\mathrm{BaTcO_3}$ ($w = 2.0$ eV) associated with the enhanced t_{2g}-p hybridization in the 3 eV wide t_{2g} band around -5.5 eV explains the larger J_1 and the corresponding larger T_N for $\mathrm{SrTcO_3}$ and $\mathrm{BaTcO_3}$. At this point a fundamental question naturally arises: Why the Tc-O hybridization increases along the $R\mathrm{TcO_3}$ series when r_R get larger?

In order to answer to this question we analyze the coupling between the structural changes, caused by the substitution of Ca with bigger isovalent atoms (Sr and Ba), and the electronic and magnetic properties, as exemplified in Fig. 3. We recall, that the most significant effects on the crystal structure caused by increasing r_R are (i) the volume enhancement, (ii) the quenching of the JT distortions $Q_2$and Q_3, and (iii) the decrease of the cooperative rotation of the $\mathrm{TcO_6}$ octahedra represented by the Tc $-\widehat{\mathrm{O}}-$ Tc bond angles. The angles Tc $-\widehat{\mathrm{O1}}-$ Tc and Tc $-\widehat{\mathrm{O2}}-$ Tc are crucial quantities to explain the evolution of the SE interactions and of the magnetic ordering temperature. In fact, the monotonic increase of the Tc $-\widehat{\mathrm{O}}-$ Tc bond angles (in brief the average between Tc $-\widehat{\mathrm{O1}}-$ Tc and Tc $-\widehat{\mathrm{O2}}-$ Tc; see Fig. 3) leads to the progressive rectification of the NN superexchange paths. This generates, in a tight-binding framework, an enhanced Tc-t_{2g}/O-p hybridization, as confirmed by the DOS (see Fig. 2). As displayed in Fig. 3, T_N steeply increases from $\mathrm{CaTcO_3}$ (750 K) to $\mathrm{SrTcO_3}$ (1135 K) as a consequence of the observed larger change in Tc $-\widehat{\mathrm{O}}-$ Tc, which goes from 151° to 167°. When moving from $\mathrm{SrTcO_3}$ to $\mathrm{BaTcO_3}$ (1218 K) the rise of T_N is weaker due to a smaller change of Tc $-\widehat{\mathrm{O}}-$ Tc (from 167° to 179°) and to a further reduction and sign change in J_2. Analoggously with the RMnO3 perovskites, the increase of T_N for larger Tc-O-Tc angles correlates with a progressive reduction of the JT distortions (i.e., a decrease of the associated structural ordering temperature).[7]

In conclusion, we remark that our findings for the 4*d* $R\mathrm{TcO_3}$ series are consistent with the Goodenough-Kanamori rules[30] and follow the general trend observed in 3*d* $R\mathrm{MnO_3}$, namely that T_N increases by increasing the $\mathrm{Tc}-\widehat{\mathrm{O}}-\mathrm{Tc}$ angles. The remarkably different T_N's in manganites ($T_N <$ 150 K) and technetiates ($T_N >$ 750 K) can be explained with the reduced spatial extension of the 3*d* shell, which suppresses the *d*-*p* hybridization in manganites and thereby inhibits strong SE interactions. We also emphasize that the correct description of this complex class of materials can be only achieved within a beyond-local functional method such as HSE. HSE is capable of capturing the delicate balance between the SE mechanism and both the Hund's coupling (unlike local functionals, HSE provides well-defined magnetic solutions for different spin configurations) and the intra-atomic Coulomb repulsion (though substantially reduced with respect to 3*d* perovskites; the on-site Coulomb interaction survives in 4*d* technetiates and contributes to the formation of a rather large gap that local functionals seriously underestimate).

ACKNOWLEDGMENTS

This work was supported by the EU-FP7 within the EU-INDIA project ATHENA. Supercomputer time was provided by the Vienna Scientific Cluster. C.F. acknowledges grant support from the CAS (Fellowship for Young International Scientists) and the NSFC (Grant No. 51050110444). We are grateful to B.-J. Kennedy for sharing with us the unpublished low-temperature structural data.

*Corresponding author: cesare.franchini@univie.ac.at

[1] O. Muller, W. B. White, and R. Roy, J. Inorg. Nucl. Chem. **26**, 2075 (1964).
[2] E. E. Rodriguez *et al.*, J. Am. Chem. Soc. **129**, 10244 (2007).
[3] E. E. Rodriguez *et al.*, Inorg. Chem. **47**, 6281 (2008).
[4] E. E. Rodriguez *et al.*, J. Mater. Chem. **21**, 1496 (2011).
[5] M. Avdeev *et al.*, J. Am. Chem. Soc. **133**, 1654 (2011).
[6] E. E. Rodriguez, F. Poineau, A. Llobet, B. J. Kennedy, M. Avdeev, G. J. Thorogood, M. L. Carter, R. Seshadri, D. J. Singh, and A. K. Cheetham, Phys. Rev. Lett. **106**, 067201 (2011).
[7] T. Kimura, S. Ishihara, H. Shintani, T. Arima, K. T. Takahashi, K. Ishizaka, and Y. Tokura, Phys. Rev. B **68**, 060403(R) (2003).
[8] K. Yamauchi, F. Freimuth, S. Blügel, and S. Picozzi, Phys. Rev. B **78**, 014403 (2008).
[9] A. D. Becke, J. Chem. Phys. **98**, 1372 (1993)
[10] D. Landau and K. Binder, *A Guide to Monte Carlo Simulations in Statistical Physics* (Cambridge University Press, Cambridge, England, 2000).
[11] K. Maiti and R. S. Singh, Phys. Rev. B **71**, 161102(R) (2005).
[12] J. Heyd, G. E. Scuseria, and M. Ernzerhof, J. Chem. Phys. **118**, 8207 (2003); **124**, 219906(E) (2006).
[13] P. E. Blöchl, Phys. Rev. B **50**, 17953 (1994).
[14] G. Kresse and D. Joubert, Phys. Rev. B **59**, 1758 (1999).
[15] G. Kresse and J. Furthmüller, Phys. Rev. B **54**, 11169 (1996).
[16] G. Kresse and J. Furthmüller, Comput. Mater. Sci. **6**, 15 (1996).
[17] The value of the mixing parameter $a = 0.1$ is reduced with respect to the standard value (0.25) since self-interaction error are considered to be smaller in 4*d* transition metal oxides. See Ref. 11.
[18] C. Franchini, G. Kresse, and R. Podloucky, Phys. Rev. Lett. **102**, 256402 (2009).
[19] J. B. A. A. Elemans, B. van Laar, K. R. van der Veen, and B. O. Loopstra, J. Phys. Chem. Solids **3**, 238 (1971).
[20] B. J. Kennedy (private communications).
[21] E. Pavarini and E. Koch, Phys. Rev. Lett. **104**, 086402 (2010).
[22] A. Filippetti and N. A. Hill, Phys. Rev. B **65**, 195120 (2002).
[23] S. F. Matar, Prog. Solid State Chem. **31**, 239 (2003).
[24] G. Trimarchi and N. Binggeli, Phys. Rev. B **71**, 035101 (2005).
[25] Xing-Qiu Chen, C. L. Fu, C. Franchini, and R. Podloucky, Phys. Rev. B **80**, 094527 (2009).
[26] G. Fischer, M. Dane, A. Ernst, P. Bruno, M. Lueders, Z. Szotek, W. Temmerman, and W. Hergert, Phys. Rev. B **80**, 014408 (2009).
[27] X. Wan, Q. Yin, and S. Y. Savrasov, Phys. Rev. Lett. **97**, 266403 (2006).
[28] P. W. Anderson, Phys. Rev. **115**, 2 (1959).
[29] J. H. Van Vleck, J. Chem. Phys. **9**, 85 (1941).
[30] J. B. Goodenough, Phys. Rev. **100**, 564 (1955); J. Kanamori, J. Phys. Chem. Solids **10**, 87 (1959).